DOI 10.1007/s11182-022-02704-3
*Russian Physics Journal, Vol. 65, No. 5, September, 2022 (Russian Original No. 5, May, 2022)*

# ACTIVATION PRODUCT DISTRIBUTION IN IRRADIATED GRAPHITE

**A. O. Pavliuk,[1] S. G. Kotlyarevsky,[1] R. I. Kan,[1] A. G. Volkova,[2] and E. V. Zakharova[2]**

UDC 621.039.75

*The paper focuses on the $^{14}C$, $^{36}C1$, and $^{60}Co$ radionuclide distribution in graphite stacks and blocks, which play a crucial role in the decommission of uranium-graphite reactors. The shutdown uranium-graphite reactor ADE-5 provides an access to the graphite stack for the removal of graphite blocks. New interpretations are suggested for the radionuclide distribution in bulk graphite stacks based on testing results of graphite blocks removed from the uranium-graphite reactor ADE-5 in 2018.*

**Keywords:** decommission, irradiated graphite, uranium-graphite reactor, nugget effect, activation products, nuclide vector.

## INTRODUCTION

By now, over 100 power and production uranium-graphite reactors have been built throughout the world. A high percentage of uranium-graphite reactors belongs to the Russian Federation, Great Britain, USA, France. There are already ~250,000 tons of irradiated graphite in the world, and this is a global problem, which is being solved at the international level within the frame of various programs and projects [1, 2]. Special attention is given to the graphite characterization due to the presence of long-lived activation products in graphite, including $^{14}C$, $^{36}C1$, $^{60}Co$ radionuclides. Information about the radionuclide content in graphite is important for the development of dismantling techniques of the graphite stack, nuclear waste disposal, deactivation and processing [3−8].

AO "Pilot and Demonstration Center for Decommissioning of Uranium-Graphite Nuclear Reactors" (Seversk, Russia) is currently involved in trying out the technology of the graphite stack dismantling, which provides an access to the graphite stack and removal of graphite blocks to investigate them and analyze the results obtained.

This paper studies the graphite stack of the decommissioned uranium-graphite reactor ADE-5 and removed graphite blocks. The obtained results are used to analyze the distribution of the most important radionuclides in the reactor, scilicet: detailed distribution of the key radionuclides $^{14}C$, $^{36}C1$, $^{60}Co$ throughout the volume of individual graphite blocks and graphite stack as a whole; the range of radionuclide concentration; determination of distribution parameters of radionuclides in graphite blocks and stack to interpret mechanisms of this distribution.

## 1. FORMATION OF RESIDUAL RADIONUCLIDES IN IRRADIATED GRAPHITE

The world experience [1, 2] as well as this work show that in general case, the isotope composition, activity, and distribution parameters of radionuclides in uranium-graphite reactors determine the following processes. Neutron

[1] JSC "Pilot and Demonstration Center for Decommissioning of Uranium-Graphite Nuclear Reactors", Seversk, Russia, e-mail: pao@dnrc.ru; ksg@dnrc.ru; kri@dnrc.ru; [2]Institute of Physical Chemistry and Electrochemistry of the Russian Academy of Sciences, Moscow, Russia, e-mail: anna.agv@yandex.ru; zakharova@ipc.rssi.ru. Translated from Izvestiya Vysshikh Uchebnykh Zavedenii, Fizika, No. 5, pp. 63–72, May, 2022. Original article submitted January 25, 2022.

 

activation of atoms of chemical elements (both primary and impurity) in non-irradiated graphite; activation of atoms of chemical elements (both primary and impurity) in circulated media (nitrogen, water) and retained in the graphite structure during the reactor operation; activation and further corrosion of constructional steelworks and cooling circuit with successive formation of corrosion products on the graphite stack parts during the reactor operation; cases of fuel egress in the graphite stack, long-term irradiation of spilled fuel, and radionuclide dispersal, and fuel source radionuclides releasing during remediation of consequences of such cases and a successive impact of operational factors on uranium-graphite reactors.

The radionuclide accumulation in irradiated graphite enables their complex distribution in the bulk graphite stack and individual graphite blocks. The distribution of some radionuclides, including long-lived $^{14}C$ and $^{36}C1$ and fuel source isotopes, is individual for each radionuclide or their group and can be determined not only by the irradiation parameters, but also by other factors. These factors play a critical role in the spatial distribution of different radionuclides and are as follows. Distribution and fixation of impurity atoms of chemical elements in the structure of non-irradiated graphite determined by the initial raw material, production process, and graphite cleaning; distribution and fixation of one type of radionuclides formed or localized from outside in different channels; developed porous structure of graphite; distribution and fixation of radionuclides in the graphite structure associated with such operating conditions as circulated media (nitrogen, water), coolant leakage, graphite stack reflooding, penetration of the fuel element material in the graphite stack.

Generalizing the research results [3, 4] concerning irradiated graphite in Russian uranium-graphite reactors, the key radionuclides in graphite stacks can be divided into several groups:

– $^{14}C$, $^{36}Cl$, $^{3}H$, $^{60}Co$ activation products of impurity elements in initial graphite;

– $^{14}C$ isotope of gas nitrogen;

– $^{60}Co$ and Eu, Ni, Zr, Nb isotopes of impurity elements of constructional steelworks and materials of the primary coolant circuit contained in their corrosion products and penetrated in graphite;

– fission products and actinides $^{137}Cs$, $^{90}Sr$, $^{154, 155}Eu$, $^{244}Cm$, $^{237}Np$ and U, Pu, Am isotopes.

A significant number of reactors in the Russian Federation are shutdown production uranium-graphite reactors, which relate to pressure-tube reactors cooled by pressurized water. Graphite stacks are employed in high purity nitrogen during the reactor power operation.

## 2. MATERIALS AND METHODS

### Sampling from graphite blocks

On the ADE-5 (calendar time in service: 43 years, holding period after uranium-graphite reactor shutdown: 12 years) shutdown in 2018, the access to the graphite stack was provided by the creation of a vertical process-oriented opening through upper steelworks and biological protection. Thus, it became possible to extract graphite blocks and collect infinite array of samples with the use of different sampling mechanisms. After the extraction of several graphite blocks through the opening, the key radionuclide content was thoroughly investigated in the volume of individual graphite blocks.

The content of radionuclides in two graphite blocks extracted from the ADE-5, was investigated in elevation and azimuth, namely: the upper block *1* 200 mm high (the elevation position matches the upper reflector position); graphite block *3* 600 mm high (the elevation position matches the upper part of the reactor core).

Graphite samples were drilled out with an 8 mm bit from the block walls, and the fragmented material taken from each sample was collected in separate tanks. For block *1*, sampling points of the fragmented material included the upper and lower end surfaces of the graphite block at a 50 mm depth; two mutually perpendicular walls (through the length and breadth of untied rows of the graphite stack) at a half-height of the graphite block (drilling through the whole wall thickness). For block *3*, sampling points of the fragmented material included the upper and lower end surfaces of the graphite block at a 50 mm depth; two mutually perpendicular walls (through the length and breadth of untied rows of the graphite stack) at five points uniformly arranged along the height of the graphite block (drilling through the whole wall thickness). Several (up to 5) samples were taken from each test portion.

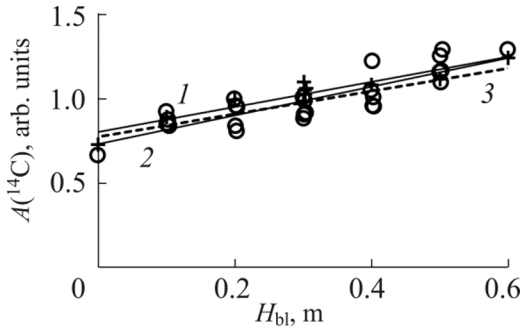


Fig. 1. Specific activity of the $^{14}C$ radionuclide over the height of extracted graphite block *3*.

**Remote sampling from graphite stack**

Core sampling from graphite blocks in the stack was performed by using a horizontal drilling system to investigate the radionuclide content in the graphite stack. Cores with the diameter 8 mm were taken from the graphite block wall at full depth (57 mm). Four or five extraction points were selected throughout the height of four graphite blocks. Five samples ~2 mm thick were cut evenly along the core length to analyze the radionuclide distribution in the depth of the graphite block walls. End samples included end surfaces of the core.

**Definition of radionuclide content**

The content of $^{14}C$ and $^{36}Cl$ radionuclides was identified in accordance with the measurement procedure of their activity in graphite blocks, using the radiometric method (industry-based instructions 001.912-2020 and 001.911-2020). The content of gamma-emitting radionuclides was determined by a gamma-ray spectrometer in accordance with the measurement procedure 15.1.6(5)-15 "Method of Measuring Countable Samples on Gamma Spectrometers".

## 3. RESULTS AND DISCUSSION

**Analysis of $^{14}C$ and $^{36}C1$ radionuclide content**

Figure 1 describes the dependence of the specific activity of the $^{14}C$ radionuclide on the height of the extracted graphite block *3* in two mutually perpendicular directions (curves *1* and *2*). On the *Y* axis, the average $^{14}C$ content is normalized for the block height at point 1.0. One can see that the difference between the experimental and approximating curves is not over 15% for some samples at all sampling points. Curves *1* and *2* demonstrate full coincidence of the $^{14}C$ radionuclide distribution over the height and the thermal neutron flux (curve *3*). The same is observed for block *1* at ~$1 \cdot 10^5$ Bq/g average specific activity of the $^{14}C$ radionuclide.

The identical distribution of the $^{14}C$ radionuclide content and thermal neutron flux is observed not only for the particular graphite blocks, but also for graphite stack as a whole. In Fig. 2, the dependence is based on the analysis of samples extracted from four blocks of the graphite stack having close values of operating parameters. Experimental points in Fig. 2 match samples from blocks *1* and *3* and samples cut from cores of graphite blocks of the stack throughout the height of the four blocks.

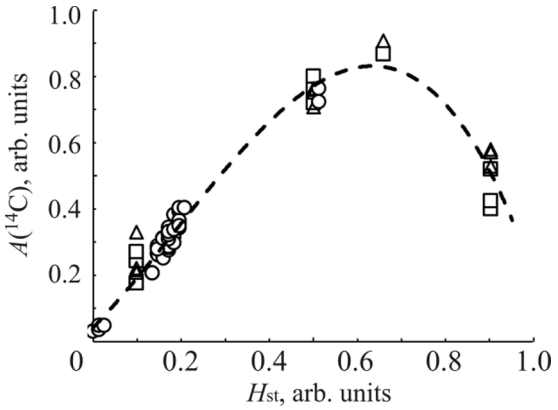


Fig. 2. Specific activity of the $^{14}C$ radionuclide over the graphite stack height. On *Y* and *X* axes, point 1.0 matches the minimum value of specific activity of the $^{14}C$ radionuclide in the graphite stack and its full height.

The core lengthwise fragmentation into separate samples provides the radionuclide distribution in the depth of the block wall. The $^{14}C$ content variation is ±20% relative to its average content in the core at each sampling point.

According to Figs. 1 and 2, the similar distribution of the $^{14}C$ content and thermal neutron flux is explained by the operation of graphite stacks in high purity nitrogen. The larger part (~70−90%) of the accumulated $^{14}C$ radionuclide releases from gas nitrogen in the channel $^{14}N(n, p)^{14}C$. During the reactor operation, this $^{14}C$ content localizes in the thin surface layer (<200 nm) of the outer surface of the graphite block, open pores, individual crystallites contacting with gas nitrogen [9–11]. The spatial distribution of the $^{14}C$ content in graphite blocks is determined only by heterogeneity of the volume fraction (relative to the surface area of the walls) of open pores in graphite and irradiation parameters. According to the experimental data on the porous structure of graphite GR-220, the volume fracture of open pores varies by ±20% relative to its mean value. This is indirectly confirmed in [12, 13]. In reactors with graphite stacks operating in carbon dioxide, the correlation with irradiation parameters is not very clear, because the main channel of the $^{14}C$ radionuclide localization is $^{14}N(n, p)^{14}C$. In this case, nitrogen atoms in graphite represent the initial impurity. The concentration of nitrogen impurities considerably varies both throughout the volume of individual graphite blocks and between them [4]. The contribution of the $^{13}C(n, \gamma)^{14}C$ reaction is much less than that of the $^{14}N(n, p)^{14}C$ reaction. This also contributes to the $^{14}C$ isotope content in the surface layer, which is higher than the average volume fraction in the graphite block. In this work, we find that the specific activity of the $^{14}C$ radionuclide in graphite samples obtained after the removal of the thin (~0.1−0.2 mm) layer from the block sides, reaches ~$1.7 \cdot 10^6$ Bq/g and exceeds the average activity in the block by 2 or 2.5 times. This effect grows with decreasing thickness of the removed layer, since the $^{14}C$ radionuclide implantation occurs at a depth not exceeding 200 nm. The contribution of the higher $^{14}C$ isotope content on the block side surface to the sample activity reduces with increasing thickness of the removed layer and approaches to the mean value. This effect is also typical for graphite blocks in the RMBK-1000 reactor. In our work, the thickness of the removed layer is ~0.05 mm, whereas the $^{14}C$ content in this layer exceeds the mean value by 5−7 times.

The $^{36}C1$ isotope content is identified for the same array of graphite samples. In Fig. 3, the relative distribution of the specific activity of the $^{36}C1$ radionuclide is given for the height of the extracted graphite block *3* in two mutually perpendicular directions (curves *1* and *2*). On the *Y* axis, the average $^{36}C1$ content of ~800 Bq/g is normalized for the block height at point 1.0.

Unlike the specific activity of the $^{14}C$ radionuclide presented in Fig. 1, the specific activity of the $^{36}C1$ radionuclide shown in Fig. 3 (curves *1* and *3*) significantly differs from the thermal neutron flux (curve *2*). The spatial distribution of the $^{36}C1$ radionuclide in block *1* is similar to that in block *3*. In block *1*, the average specific activity of the $^{36}C1$ radionuclide is ~300 Bq/g.

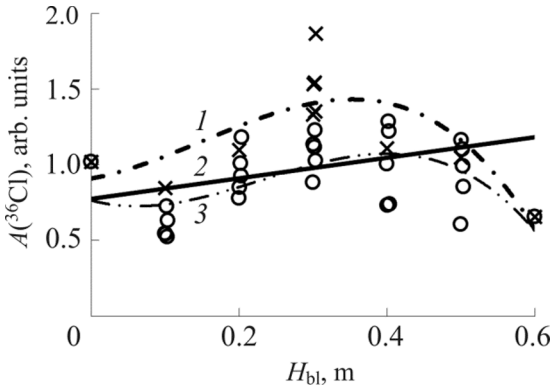


Fig. 3. Relative distribution of specific activity of the $^{36}$C1 radionuclide along the height of extracted graphite block *3*.

It should be noted that the main values of the specific activity of the $^{36}$C1 radionuclide for 5 samples selected randomly at each sampling point, varies by ±30% relative to its mean value. In measuring the $^{36}$C1 isotope content in samples cut lengthwise from the core, the variation values obtained for the $^{36}$C1 radionuclide content in the wall thickness, are more significant than for the $^{14}$C radionuclide. Some of the samples manifest significant deviation up to +250% (nugget effect) from the mean value. If we exclude the data characterized by this significant deviation, the average content of the $^{36}$C1 radionuclide in the wall thickness ranges between ±40 and 50% relative to its mean value. This can be explained by the fact that drilling through the entire wall thickness leads to averaging the radionuclide content in the volume of the drilled area due to a mixing of the fine fraction appearing during drilling.

The specific activity of the $^{36}$C1 radionuclide ranges within ±50% for the block thickness. This deviation can reach 90% for unit experimental values (see Fig. 3), which considerably exceeds the measurement accuracy of ~15%.

Figure 4 presents the distribution of the $^{36}$C1 radionuclide along the height of the graphite stack. This dependence is based on the experimental data obtained for samples from four graphite blocks having almost the same operating parameters. According to Fig. 4, no clear correlation is observed for the parameters of neutron irradiation for both individual graphite blocks (see Fig. 3) and graphite stack as a whole. The general tendency is observed for the decrease in the $^{36}$C1 content nearby the upper and lower boundary of the graphite stack. As can be seen from Fig. 4, most of the experimental data points range within ±90% (curves *1* and *3*) relative to the approximating curve *2* and significantly exceed the spatial distribution bandwidth of the thermal neutron flux.

One can see that the $^{36}$Cl content largely depends on the content variation of impurity parent atoms in the volume of and between the individual graphite blocks.

Bushuev *et al*. [4] identified the chlorine impurity content in non-irradiated graphite GR-220 applied in production uranium-graphite reactors, including the ADE-5. A wide range of its volume fraction ($0.62\cdot10^{-4}$–$9.8\cdot10^{-4}$ wt.%) was demonstrated both in the volume of and between individual graphite blocks.

It is worth noting that unlike the $^{14}$C content, the content of the $^{36}$Cl radionuclide in samples obtained after the removal of the surface layer from the sides of block *3*, tends to decrease in this surface layer (~350−400 Bq/g) compared to its average content of ~800 Bq/g in the bulk graphite block.

**Mechanisms of the $^{36}$Cl isotope distribution in graphite blocks**

Generally, the experimental data confirm that $^{36}$Cl isotopes are present in graphite in localized regions (nugget effect) [14, 15], that enables a significant variation in its specific activity. Different interpretations of the nugget effect are being currently considered, including complex processes in the crystal lattice, which facilitate the formation of localized regions with $^{36}$Cl isotopes during the reactor operation.

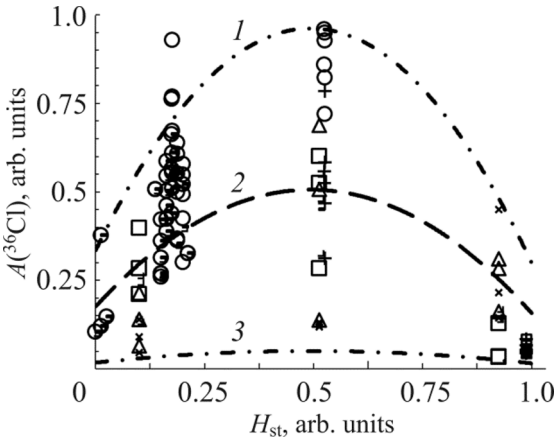


Fig. 4. Relative distribution of specific activity of the $^{36}C1$ radionuclide in graphite block along the height of the graphite stack. On *Y* and *X* axes, point 1.0 matches the maximum value of specific activity of the $^{14}C$ radionuclide in the graphite stack and its full height.

In this work, we suggest to interpret the mechanisms of the $^{36}Cl$ isotope formation in graphite blocks based on the analysis of the graphite production with regard to its highly porous structure.

As noted earlier, the primary reaction of the $^{36}Cl$ formation in irradiated graphite of uranium-graphite reactors, is $^{35}Cl(n, \gamma)\ ^{36}Cl$ ($\sigma = 43$ barn). According to [16], the chlorine impurity in graphite is conditioned by thermochemical cleaning in halogen-containing gas medium at a simultaneous exposure to high temperatures ranging between ~2500 and 3000°C. The GR-220 graphite production for uranium-graphite reactors utilizes chlorine as a halogen. The chlorine-containing gas medium is provided by the introduction of easily dissociating chlorine compounds, usually freons, in the volume to be heated. Freon-10 ($CCl_4$) is mostly used in graphite of production uranium-graphite reactors.

Thermochemical cleaning provides the formation of chlorinated volatile compounds with major impurities containing in graphite parts after graphitation and their release outside graphite parts from pore channels into the gas medium. In [15, 17], it is shown that at temperatures higher than 2000°C, the mass transfer in pores is the time limiting process of the impurity removal.

The final phase of thermochemical cleaning of graphite in production uranium-graphite reactors, is the substitution of halogen-containing gas medium and reaction products (chlorine compounds) by the nitrogen/argon gas flow in the heated volume, which is neutral relative to graphite, and cooling of graphite blocks in the furnace. Halogen-containing gas medium and reaction products are forcedly removed only from the furnace. Halogen-containing gas medium and reaction products (chlorine and impurities) remained in graphite parts, release from their surface through a gradual substitution by the gas fed in the furnace in intercommunicating pores. In other words, this process is the residual gas flow, including chlorine and chlorine compounds, in the system of intercommunicating pores and its substitution by the gas.

According to [18, 19], open pores in the bulk graphite is a developed structure with intercommunicating pore channels. At the same time, the open pore system in graphite is a uniform volume. A three-dimensional model of the graphite structure presented in [19], demonstrates the main pores of the first order, which intercommunicate with each other and with the graphite surface. Pores of the second and third orders develop from the main pores and are characterized by a considerably small size. Most of them are one-side open pores. When the gas medium substitutes another one, significantly differing in the density, properties, and fluid dynamics parameters, dead (in relation to the substituted gas medium) regions and formations inevitably appear in this pore system. The regions of chlorine and chlorine compound stagnation are schematically illustrated in Fig. 5, when halogen-containing gas medium is substituted by nitrogen or argon. In particular, since the density of gaseous chlorine is 2.6 and 1.8 times higher than the

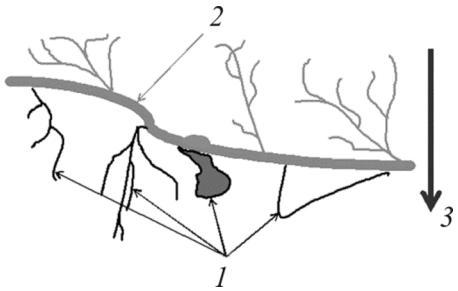


Fig. 5. Regions of chlorine and chlorine compound stagnation during halogen-containing gas medium substitution by nitrogen/argon: *1* – one-side open pores or pore channel branches with downward directed second and third order pores; underneath blind regions between adjacent grains; *2* – pore channel regions below the main pore channel, which shunt its part and have no connection with channels below; *3* – gravity direction.

density of nitrogen and argon respectively, dead regions and formations may represent a porous structure being a potential well in relation to the gravity direction.

The exchange between substituting and substituted gases in dead regions is difficult because of the higher density of the substituting gas, that creates conditions for a higher residual concentration of chlorine and its compounds. Further cooling provides the accumulation of chlorine and its compounds (already formed, forming during cooling, and those placed in air) in the graphite structure and on its surface and also their penetration in the surface layers of the graphite crystal structure [20]. The amount of chlorine and chlorine compounds localized in these regions and their spatial distribution throughout the graphite block depends on the following factors:

– parameters of the porous graphite structure and their variation over the graphite blocks and between them;

– type and composition of the raw material;

– sequence and parameters of the graphite block manufacturing process;

– types of halogen-containing gas medium and substituting gas used in thermochemical cleaning;

– graphite part orientation in the furnace during thermochemical cleaning;

– gas temperature and pressure, their gradients and dynamics during thermochemical cleaning in the furnace and bulk graphite part;

– thermo- and fluid dynamics parameters of substituting gas flows in the furnace.

We have already experimentally determined that in the volume of individual graphite blocks, the $^{36}Cl$ content ranges within ±50% of the average content in the block. The $^{36}Cl$ content in individual graphite samples can exceed the mean value by several times. Most likely, a non-uniform $^{36}Cl$ distribution over the individual graphite block, is determined by the variational parameters of concentration and geometrical parameters of formations in the graphite porous structure, in which residual chlorine and its compounds localize during thermochemical cleaning. In our early research [9], the volume fraction of open pores in graphite for production uranium-graphite reactors, is ±20% of the average content for the pore size ranging between 5 and 10 mm.

It is likely that the range of the variational parameters of concentration and geometrical parameters of formations in the graphite porous structure accumulating chlorine and its compounds, correlates with the volume fraction of open pores. According to [9], the mean diameter of pore channels is ~18 μm for graphite GR-220. The pore size distribution depends on that approaching to the Poisson distribution, that also determines the parameter range of the geometry of these formations. Totally, these effects can determine a ±50% variation in the $^{36}Cl$ content for the main volume part of individual graphite blocks.

At the same time, there are cavities in the graphite porous structure [9, 19] having the size anomalously larger (up to several tenths of millimeter) than that of the usual pore size. When such a cavity has properties of a potential well

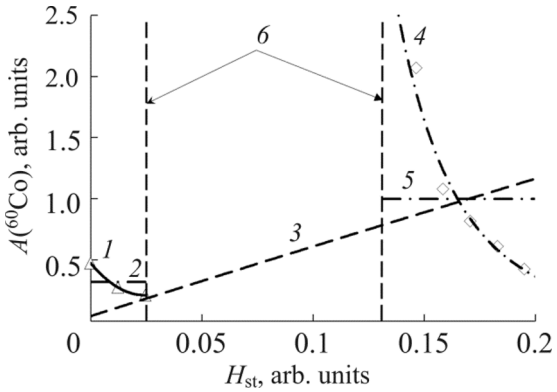


Fig. 6. Relative distribution of specific activity of the $^{60}$Co radionuclide over the height of extracted graphite blocks *1* and *3*.

in relation to the gravity, it can accumulate much more chlorine and its compounds than the rest graphite bulk, thereby providing the formation of a localized volume with the higher $^{36}$Cl content. This explains the experimental data obtained for graphite samples with the anomalously large $^{36}$Cl content (nugget effect).

As can be seen from Fig. 3, the $^{36}$Cl content distribution along the graphite block height tends to decrease at its end faces. The $^{36}$Cl content in graphite samples obtained after the removal of the thin surface layer from the sides of block *3*, tends to decrease in this surface layer (~350−400 Bq/g) compared to its mean value of ~800 Bq/g in the bulk graphite block. These results indicate that the gas exchange is more intensive than in deep layers during the substitution of chlorine and its compounds from pore channels by nitrogen or argon after thermochemical cleaning.

**$^{60}$Co content in graphite blocks**

According to our experiments, the content of $^{60}$Co and $^{36}$Cl in graphite blocks mostly depends on the concentration range of impurity parent atoms determined by the raw material composition, graphite technology, and operation conditions of production uranium-graphite reactors. It is found [4] that non-irradiated graphite GR-220 contains a wide range of cobalt impurities ($0.7\cdot10^{-7}$–$3.8\cdot10^{-6}$ wt.%) both throughout the volume of individual graphite blocks and between them. This provides the spatial distribution of the $^{60}$Co content averaged by the volume of individual graphite blocks in the graphite stack similar to the spatial distribution of the $^{36}$Cl content (see Fig. 4).

The spatial distribution in individual graphite blocks is described by the specific properties of the $^{60}$Co radionuclide. The surface layer of graphite blocks is usually high in $^{60}$Co due to its dissipation by water and vapor-water medium in the case of the coolant leakage and setting on the graphite surface. This $^{60}$Co content localizes in corrosion products of materials contained in the primary coolant circuit and steelworks. The $^{60}$Co radionuclide can also disperse in the graphite stack in the form of corrosion products of the molten material of process-oriented channels and tube shells of fuel elements formed during the reactor operation. Thus, the $^{60}$Co content in graphite samples obtained by the removal of the thin surface layer from the lateral surface of block *3*, is 10 times higher ($1\cdot10^5$ Bq/g) than its mean value in the bulk graphite block.

Specific activity of the $^{60}$Co radionuclide over the height of removed graphite blocks *1* and *3* is presented in Fig. 6. On the *Y* axis, point 1.0 matches the average specific activity (~$7\cdot10^3$ Bq/g) of the $^{60}$Co radionuclide in the bulk graphite block. Dashed lines *6* indicate the lower and upper boundaries of blocks *1* and *3*, respectively, which correspond to their arrangement along the graphite stack height.

As can be seen from Fig. 6, the specific activity decreases by about 2 times for block *1* (curve *1*) and about 7 times for block *3* (curve *4*), from the upper to the lower boundary of graphite blocks. Levels *2* and *5* match the average content of $^{60}$Co in blocks *1* and *3*, respectively. With respect to the “mirror” behavior of thermal neutron flux (curve *3*)

at these points, the concentration difference of the initial impurity atoms is higher along the block height. Since the spatial distribution is complex for both graphite blocks, i.e., monotonically decreases downwards, we can assume that such a distribution is not random and occurs at the production stage and/or during thermochemical cleaning of graphite parts. This distribution probably occurs during thermochemical cleaning and substitution of chlorine and its compounds by nitrogen or argon after thermochemical cleaning. This occurs if cobalt chloride compounds drain down by the force of gravity relative to the position of the graphite part in the thermal chamber and delay in the porous structure as gas flows forward. Another reason is the vertical gas flow in pores, from bottom to top due to a convection produced by the heated surface of the thermal chamber with graphite parts on it.

In addition to the $^{60}$Co radionuclide, the concentration is determined for $^{134}$Cs, $^{137}$Cs, $^{133}$Ba radionuclides which emit gamma radiation. The higher content of these radionuclides is observed in the surface layer, *viz*. 3 times higher for $^{134}$Cs, 200 times higher for $^{137}$Cs, and 4 times higher for $^{133}$Ba than their average content in the bulk graphite block. It should be noted that $^{134}$Cs and $^{133}$Ba radionuclides are present in graphite as impurity activation products and settle on the graphite surface as fission products from spilled fuel fragments. In this case, the $^{137}$Cs radionuclide settles on the graphite surface as a fission product only.

## CONCLUSIONS

This research suggested the explanation for the spatial distribution of the key radionuclides $^{14}$C, $^{36}$C1, $^{60}$Co in irradiated graphite of uranium-graphite reactors. It was shown that the shape of the spatial distribution of thermal neutron flux in the graphite stack determined the spatial distribution of the $^{14}$C content. Therefore, the spatial distribution of the $^{14}$C content in the graphite stack and blocks was described by the function connecting its concentration with the block position in the graphite stack. The content variation of the initial impurity atoms in graphite determined the content of $^{36}$C1 and $^{60}$Co radionuclides. It was thus advisable to describe their distribution in the graphite stack by statistical distribution functions.

It was impossible to use the scaling factor method to determine the content of $^{14}$C and $^{36}$C1 radionuclides (difficult to measure beta-emitters) in graphite. That was because the correlation between the dynamics of their accumulation and neutron irradiation parameters with gamma-emitting radionuclides ($^{60}$Co and others) typical for irradiated graphite, was ambiguous. At the same neutron irradiation parameters, the significant variation (up to several orders of magnitude) was observed for the ratio between determined ($^{14}$C and $^{36}$C1) and reference ($^{60}$Co and others) radionuclides.

From a practical perspective, the typical properties of the spatial distribution and activity levels of the key radionuclides in graphite of production uranium-graphite reactors, do not significantly differ from graphite in the RMBK-1000 reactor after its shutdown. This fact can become the basis for decommission of production uranium-graphite reactors using on-site disposal option to support RMBK-1000 irradiated graphite disposal in near-surface burial sites.

This work was financially supported by Rosatom State Nuclear Energy Corporation and carried out in the frame of Contact No. N.4d.241.20.19.1008.

## REFERENCES

1. IAEA TECDOC-1790, IAEA, Vienna (2015).
2. A. Wickham, H.-J. Steinmetz, P. O'Sullivan, and M. I. Ojovan, Journal of Environmental Radioactivity, **171**, 34−40 (2017).
3. A. N. Dorofeev, E. A. Komarov, E. V. Zakharova, A. G. Volkova, I. I. Linge, A. Yu. Ivanov, *et al*., Radioaktivnye otkhody, No. 2 (7), 18−30 (2019).
4. A. V. Bushuev, A. F. Kozhin, E. V. Petrova, *et al*., Radioactive Reactor Graphite [in Russian], National Research Nuclear University MEPhI, Moscow (2015).
5. E. S. Paderin, A. A. Sheshin, and K. E. Orlov, Radioaktivnye otkhody, No. 3 (8), 69−73 (2019).

6. Yu. A. Pokhitonov, Radiokhimiya, **62**, No. 3, 183–194 (2020).
7. N. A. Girke, A. V. Bushuev, A. F. Kozhin, E. V. Petrova, T. B. Aleeva, and V. N. Zubarev, Atom. Energy, **112**, No. 1, 63–66 (2012).
8. N. A. Girke, A. V. Bushuev, A. F. Kozhin, *et al*., Yad. Fiz. Inzhiniring, **3**, No. 3, 203 (2012).
9. A. A. Shiryaev, A. G. Volkova, E. V. Zakharova, *et al*., Radiokhimiya, **60**, No. 6, 564−570 (2018).
10. B. A. Gurovich and K. E. Prikhodko, Radiat. Eff. Defect S., **154**, No. 1, 39−60 (2001).
11. J. H. W. Simmons, Radiation Damage in Graphite, Pergamon Press, Oxford (1965).
12. M. P. Metcalfe and R. W. Mills, Ann. Nucl. Energy, **75**, 665−671 (2015).
13. J. Comte, C. Guy, L. Gosmain, and S. Parraud, Determining the Porosity and Water Impregnation in Irradiated Graphite, J. Nucl. Mater., 528, doi.org/10.1016/j.jnucmat.2019.151816.
14. G. O. Nicaise and B. Poncet, Kerntechnik, **81**, No. 5, 565−570 (2016).
15. E. V. Bespala, A. O. Pavlyuk, S. G. Kotlyarevskii, and I. Yu. Novoselov, Poverkhnost'. Rentgenovskie, sinkhrotronnye i neitronnye issledovaniya, No. 2, 63–71 (2020).
16. H. Tobias and A. Soffer, Carbon, **23**, No. 3, 281–289 (1985).
17. S. E. Vyatkin, *et al*., Nuclear Graphite [in Russian], Atomizdat, Moscow (1967).
18. Yu. S. Virgil'ev, Khim. Tverd. Topl. (Moscow), No. 5, 102−105 (1973).
19. J. J. Kane, A. C. Matthews, W. D. Swank, and W. E. Windes, Carbon, **166**, 291–306 (2020).
20. D. Pasquevich, Thermochim. Acta, **167**, 91–98 (1990).